

Phase retrieval from single biomolecule diffraction pattern

Shiro Ikeda

*The Institute of Statistical Mathematics,
10-3 Midori-cho, Tachikawa, Tokyo 190-8562, Japan**

Hidetoshi Kono

*Japan Atomic Energy Agency, 8-1-7 Umemidai,
Kizugawa, Kyoto 619-0215, Japan†*

(Dated: Ver. 1.2 on 9/Feb/2011)

Abstract

A new phase retrieval method for noisy x-ray diffraction imaging is proposed. Conventional phase retrieval methods effectively solve the problem for high signal-to-noise ratio measurements, but would not be sufficient for single biomolecular imaging which is expected to be realized with femto-second x-ray free electron laser pulses. The new phase retrieval method is based on the Bayesian statistical approach. The method does not need to set the object boundary constraint that is required by the commonly used hybrid input-output method, instead a sparse prior is used for the object estimation, and we call it SPR (sparse phase retrieval) method. The simulation results demonstrate that the SPR method can reconstruct the object efficiently under a realistic condition.

* shiro@ism.ac.jp

† kono.hidetoshi@jaea.go.jp

X-ray free electron lasers (XFELs) can potentially provide us a novel mean to determine the three-dimensional (3D) structure of biomolecules from the diffraction data of single molecules [1, 2]. Conventionally, x-ray crystallography has been the principal tool to determine high-resolution 3D structures of proteins, nucleic acids, and their complexes. However, a critical process is the crystallization. A sufficiently large crystal must be prepared. It is known that about 40% of biomolecules, particularly membrane proteins, do not crystallize. The coherent x-ray diffraction imaging by XFELs does not require a crystal and will change such a situation.

In order to realize the single molecule imaging, a straightforward scenario has been proposed and demonstrated [3–5]. Firstly, a series of single molecules with the same structure are injected in vacuum and exposed to the short pulse x-ray beam. The diffraction image of the molecule with unknown orientation is recorded before radiation-induced structural degradation. This process is repeated until sufficient number of images are recorded. The diffraction data are then classified into groups according to the orientations of the molecule and averaged to improve the signal-to-noise ratio. Next, the relative orientations of the classes are determined to assemble a 3D coherent diffraction pattern in reciprocal space. Finally, the 3D electron density of the molecule is obtained by phase retrieval. In doing so, we have to overcome critical limitations for each process due to the small number of photons scattered by a single molecule even though x-ray beams that linac coherent light source (LCLS) has started to commission give us illumination which is around 10^9 times brighter ($\sim 10^{19}$ photons/pulse/mm²) than that of current synchrotrons [6].

Here, we propose a new approach, the sparse phase retrieval (SPR) method, for retrieving phases of diffraction data which will be obtained by XFELs. The method is based on the Bayesian statistics. The diffraction pattern is described with the Poisson distribution and the sparse prior is employed. This combination is effective for this problem and is distinct from other Bayesian approaches proposed for different phase retrieval problems [7, 8]. Compared to the widely used hybrid input-output (HIO) method [9], the SPR method is more robust against photon noise and the support region is not required.

Let $f(x, y) \geq 0$ be the electron density of a molecule projected onto a two-dimensional (2D) plane. In this letter, we consider the 2D case, which corresponds to the phase retrieval of a single diffraction image, but the proposed SPR method can be easily applied to the 3D case. The coordinate is discretized, that is, $x, y = 1, \dots, M$. We introduce the following

notation

$$\begin{aligned}\mathbf{f} &= \{f(x, y)\} = \{f_{xy}\} = \{f_{11}, \dots, f_{MM}\} \\ \mathbf{F} &= \{F(u, v)\} = \{F_{uv}\} = \{F_{11}, \dots, F_{MM}\},\end{aligned}$$

where, \mathbf{F} is the Fourier transform of \mathbf{f} defined as follows,

$$F_{uv} = (\mathcal{F}(\mathbf{f}))_{uv} = \frac{1}{M} \sum_{x,y} f_{xy} \exp\left(\frac{2\pi i(ux + vy)}{M}\right). \quad (1)$$

The coefficient of the Fourier transform differs from the commonly used $1/M^2$. We prefer the above definition because the power of \mathbf{F} and \mathbf{f} is the same.

In the idealized situation, the diffraction pattern is proportional to the power spectrum $|F_{uv}|^2$ where (u, v) corresponds to the index of the pixel. Although the phase information is lost, the density can be recovered when it is localized in a small region of the 2D space [9–11].

The reality is more complicated. For a single molecule diffraction, the flux of the x-ray laser is not sufficiently large that the number of the photons detected by each pixel of the sensor is small and noisy. This makes the reconstruction difficult. Moreover, the conventional methods may not work because the influence of the noise of the diffraction image will be distributed globally over the 2D plane. An approximate inference of the density must be computed from the limited noisy observation.

Let N_{uv} be the number of the photons detected at (u, v) of the detector. It is reasonable to assume N_{uv} is a stochastic variable. We first study the distribution of N_{uv} and consider how to recover \mathbf{f} from the observation.

The total number $N_{all} = \sum_{uv} N_{uv}$ of photons arriving at the 2D plane is a stochastic variable which follows the Poisson distribution. The expected value of N_{all} is proportional to the intensity I_X of x-ray. Assuming each N_{uv} is independent and the distribution belongs to the same family, each N_{uv} also follows a Poisson distribution. Let the expected value of N_{uv} be S_{uv} and the distribution of N_{uv} becomes

$$p(N_{uv}|S_{uv}) = \frac{S_{uv}^{N_{uv}} \exp(-S_{uv})}{N_{uv}!}. \quad (2)$$

Approximately, S_{uv} is denoted as $S_{uv} = \alpha |F_{uv}|^2 \cos^3 \theta$, where α is a positive constant and θ is the scattering angle. Because θ is a function of u and v , we further rewrite it as $\alpha |F_{uv}|^2 c_{uv}$, where $c_{uv} = c(u, v) = \cos^3 \theta$.

The Fourier transform, \mathbf{F} , is a linear function of \mathbf{f} , and the probability of \mathbf{N} , where $\mathbf{N} = \{N_{uv}\} = \{N_{11}, \dots, N_{MM}\}$, is denoted as follows

$$p(\mathbf{N}|\mathbf{f}) = \prod_{uv} \frac{(|F_{uv}|^2 c_{uv})^{N_{uv}} \exp(-|F_{uv}|^2 c_{uv})}{N_{uv}!}. \quad (3)$$

Note that the scaling of $|F_{uv}|^2$ cannot be determined only from the observed scattering pattern and α is set to 1. This scaling indeterminacy is ignored here. It will be recovered from other knowledge, such as the total energy.

In the following, we consider the density reconstruction as an estimation problem of \mathbf{f} . Commonly used estimator is the maximum likelihood estimator, which is the maximizer of $p(\mathbf{N}|\mathbf{f})$. The likelihood (3) is maximized by setting $|F_{uv}|^2 = N_{uv}/c_{uv}$, but this is not sufficient because the phase is lost. We need additional information.

As mentioned above, commonly used methods set a support region and assume $f_{xy} = 0$ outside the support [9–11]. This is effective for noiseless case, but the noise on the diffraction image affects the whole density space, and it is better to absorb the influence globally.

We employ the Bayesian statistical framework. A prior distribution is defined for the electron density \mathbf{f} and the posterior distribution is computed. Similar framework has been proposed for different types of phase retrieval problems [7, 8]. If the prior of \mathbf{f} is constant inside the support region and 0 outside, the method is essentially equivalent to the HIO method [8]. Instead, the SPR method only assumes that a lot of f_{xy} 's are 0, in other words, \mathbf{f} is “sparse,” without setting the support region.

A commonly used prior to pose the sparsity is the exponential distribution [12],

$$\pi(f_{xy}) = \rho_{xy} \exp(-\rho_{xy} f_{xy}), \quad f_{xy} \geq 0, \quad \rho_{xy} \geq 0,$$

where the hyperparameter ρ_{xy} reflects the prior belief of f_{xy} to be 0. Larger the value of ρ_{xy} , stronger the belief that f_{xy} is 0. By setting the prior of each f_{xy} independent of each other, the prior of \mathbf{f} becomes $\pi(\mathbf{f}) = \prod_{xy} \pi(f_{xy})$.

The posterior distribution of \mathbf{f} observing \mathbf{N} has the following relation,

$$p(\mathbf{f}|\mathbf{N}) \propto p(\mathbf{N}|\mathbf{f})\pi(\mathbf{f}). \quad (4)$$

The maximizer of the posterior distribution is the maximum a posteriori (MAP) estimator, and the SPR method computes the MAP estimate for the density reconstruction. The sparse prior automatically set many entries of \mathbf{f} equal to 0 without specifying the support region.

For computing MAP, it is convenient to take the logarithm of $p(\mathbf{f}|\mathbf{N})$. By collecting the terms related to \mathbf{f} , the following function is obtained,

$$\ell(\mathbf{f}|\mathbf{N}) = \sum_{uv} (N_{uv} \ln |F_{uv}|^2 - |F_{uv}|^2 c_{uv}) - \sum_{xy} \rho_{xy} f_{xy}.$$

The first summation comes from the Poisson distribution which is similar to [7]. It is different from the mean square error and maximized when $N_{uv} = |F_{uv}|^2 c_{uv}$. The second summation represents the sparse prior. Similar idea has been widely appeared in statistics, but has not been applied for the phase retrieval.

The function $\ell(\mathbf{f}|\mathbf{N})$ is a nonlinear concave function of \mathbf{f} . A gradient based algorithm is used for the MAP estimate. It is important to check which f_{xy} becomes 0 at each update step. The algorithm is shown below starting with the following relation,

$$\frac{\partial |F_{uv}|^2}{\partial f_{xy}} = \frac{2}{M} \text{Re} \left(F_{uv} \exp \left(-\frac{2\pi i (ux + vy)}{M} \right) \right).$$

By defining the inverse Fourier transform as

$$(\mathcal{F}^{-1}(\mathbf{F}))_{xy} = \frac{1}{M} \sum_{uv} F_{uv} \exp \left(-\frac{2\pi i (ux + vy)}{M} \right),$$

the derivative of $\ell(\mathbf{f}|\mathbf{I})$ becomes

$$\frac{\partial \ell(\mathbf{f}|\mathbf{N})}{\partial f_{xy}} = 2 \text{Re}(\mathcal{F}^{-1}(\mathbf{g}(\mathbf{F}; \mathbf{N})))_{xy} - \rho_{xy},$$

where $\mathbf{g}(\mathbf{F}; \mathbf{N}) = \{g_{uv}(F_{uv}; N_{uv})\}$ and

$$g_{uv}(F_{uv}; N_{uv}) = \left(\frac{N_{uv}}{|F_{uv}|^2} - c_{uv} \right) F_{uv}.$$

In order to compute the derivative of $\ell(\mathbf{f}|\mathbf{N})$, \mathcal{F} is applied to \mathbf{f} , then \mathcal{F}^{-1} is applied. Thus, the computational cost is similar to the HIO method [10].

We employed a naïve iterative updating rule for the MAP estimate of f_{xy} , $x, y = 1, \dots, M$.

$$f_{xy}^{t+1} = \max \left(0, f_{xy}^t + \eta_t \frac{\partial \ell(\mathbf{f}^t|\mathbf{N})}{\partial f_{xy}^t} \right). \quad (5)$$

The index t shows the iteration number. The “max” operation keeps f_{xy} nonnegative and the step size η_t controls the amount of the update at each step. The step size η_t is allowed to be different for each iteration.

The SPR method is tested with simulated data. The details are shown below. The diffraction data are simulated as follows. The electron density of lysozyme, a 14 kD protein,

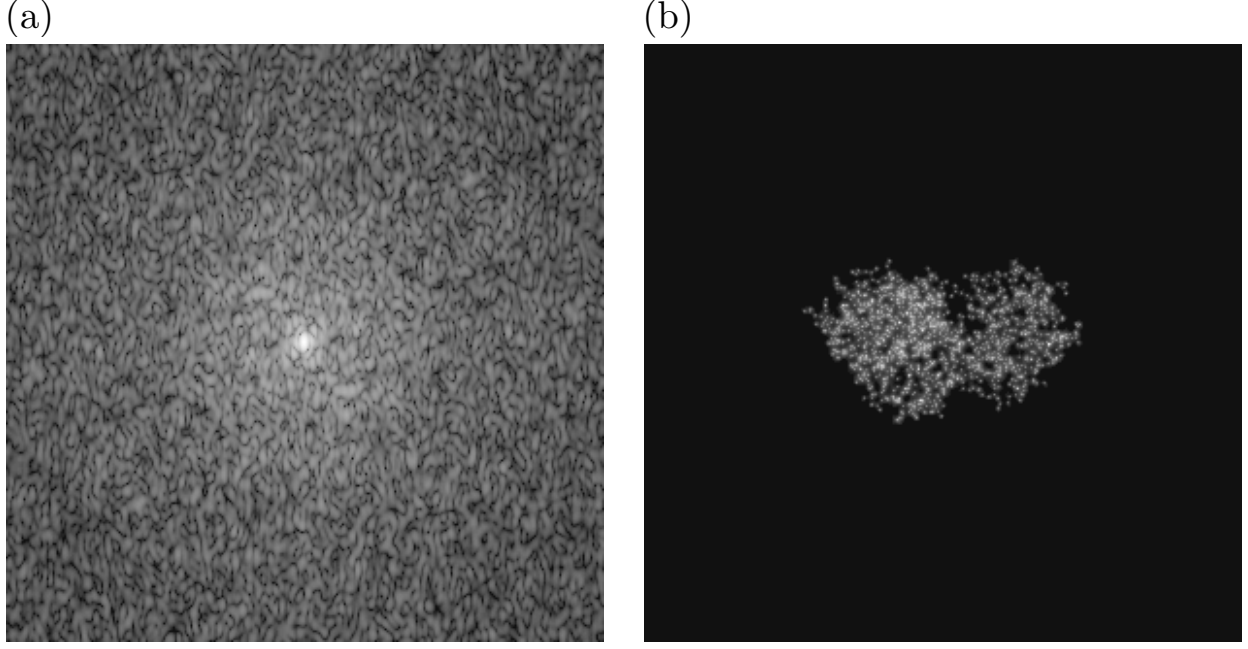


FIG. 1. (a) An ideal 2D diffraction image of lysozyme without noise, where the spacial frequency is 0.0812 nm^{-1} . (b) 2D electron density of lysozyme. Both images are 308×308 pixels.

was projected onto a 2D plane. The projected density was then Fourier transformed into reciprocal space (u, v) to simulate a diffraction image. Figure 1 shows the ideal diffraction image and the density.

We then simulated the diffraction images by converting the diffraction intensity into the number of photons per effective pixel $(\lambda/\sigma L)^2$ according to the Poisson distribution with the mean, S_{uv} , defined as follows,

$$S_{uv} = \alpha |F_{uv}|^2 c_{uv} = I r_c^2 \left(\frac{\lambda}{\sigma L} \right)^2 |F_{uv}|^2 c_{uv}.$$

Here, I is the incident x-ray flux (photons/pulse/ mm^2), r_c is the classical electron radius ($2.82 \times 10^{-12} \text{ nm}$), λ is the x-ray wave length (0.1 nm), σ is the oversampling ratio per one dimension (2), and L is the the molecule diameter (6.16 nm). The Ewald sphere curvature was ignored but this is a good approximation for small angles.

Two examples for scattered photons of x-ray fluxes with $I = 1.0 \times 10^{21}$ and 5.0×10^{21} are shown in Figs. 2(a) and 2(b), respectively. Although the fluxes are around 100 times larger than that of the current LCLS, the sizes of the molecules of interest are generally larger than lysozyme. When the size is around 1000 kD, the total number of photons arriving at the 2D plane would be in the similar range as in Fig. 2. The diffraction images are so noisy

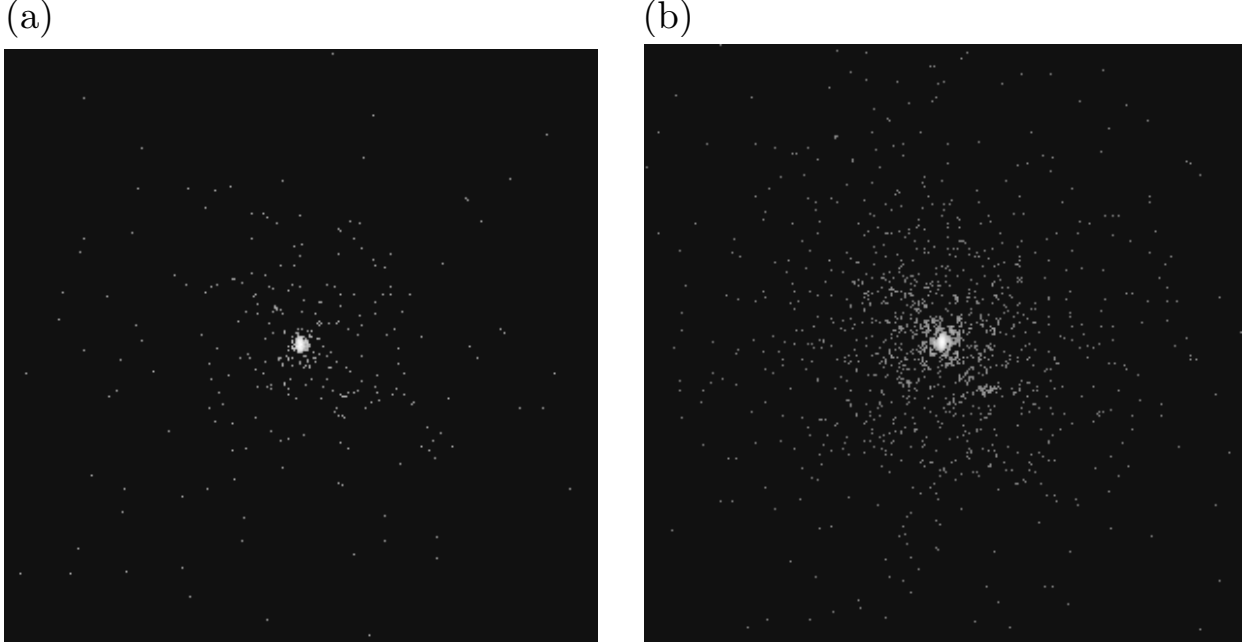


FIG. 2. Simulated diffraction images of a lysozyme protein with different x-ray fluxes I (photons/pulse/mm²). (a) $I = 1.0 \times 10^{21}$. The total number of photons is 957. (b) $I = 5.0 \times 10^{21}$. The total number of photons is 4630.

that the HIO method did not converge [13].

The SPR method was applied to the data to reconstruct the density. For the SPR method, the choice of hyperparameter ρ_{xy} is important. We assumed that high density region is around the center of the 2D plane and set ρ_{xy} as a one parameter function $\rho(\mu)_{xy}$ where

$$\rho(\mu)_{xy} = \mu w_{xy},$$

$$w_{xy} = a \left\{ \left(x - \frac{1+M}{2} \right)^2 + \left(y - \frac{1+M}{2} \right)^2 \right\} + b. \quad (6)$$

The two parameters a and b were adjusted to make w_{xy} equal to 0 at the center and 1 at the corners. This function reflects our assumption because the magnitude of the hyperparameter corresponds to the belief of f_{xy} to be 0. Compared to conventional HIO methods, where the density is set 0 outside the support region, the SPR method uses a “soft constraint,” since the density of the outer region is more likely but not necessarily 0.

We explain how the new parameter μ is used in the SPR method. In the HIO method, when the support region is not known, commonly used procedure is to start from a large region and to shrink it gradually [14]. The role of μ is similar to the region shrinking.

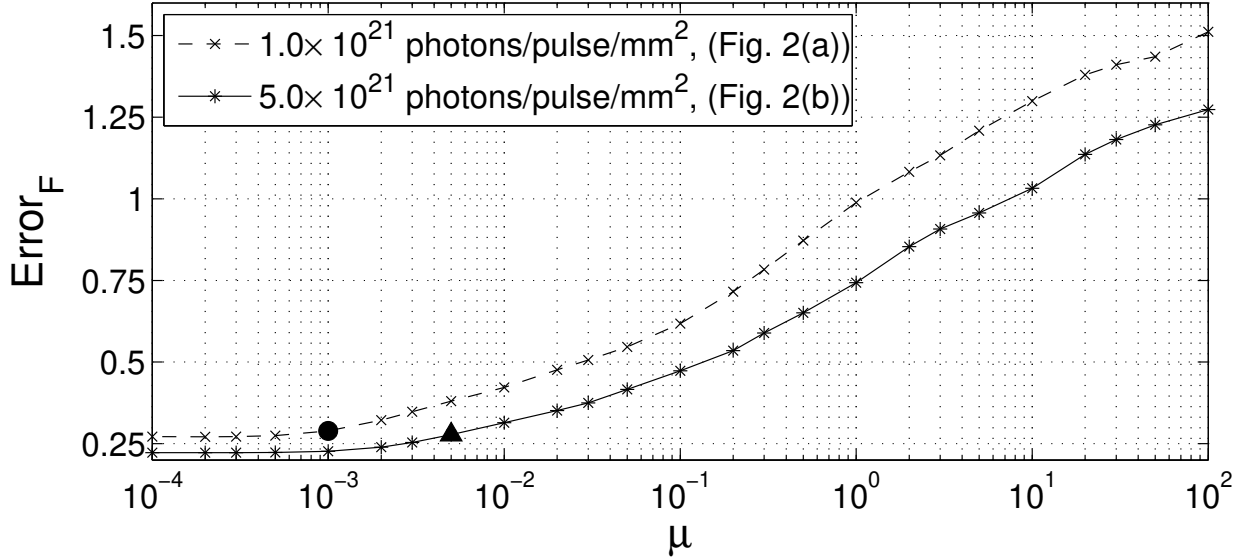


FIG. 3. The error $\text{error}_{\mathcal{F}}(\mu)$ for simulated noisy data shown in Fig. 2. The black circle and triangle on the curves correspond to the reconstructed density images of Figs. 4(c) and 4(d), respectively.

When the value of μ is large, more components of \mathbf{f} become 0. Thus, we start from a large μ and decrease it until we have a satisfactory result. Let $\hat{\mathbf{f}}(\mu)$ be the maximizer of $\ell(\mathbf{f}|\mathbf{N})$, where ρ_{xy} is $\rho(\mu)_{xy}$ (6). The following error of the estimated density $\hat{\mathbf{f}}(\mu)$ is checked for each μ

$$\text{error}_{\mathcal{F}}(\mu) = \frac{\sum_{uv} (|\hat{F}(\mu)_{uv}| c_{uv}^{1/2} - N_{uv}^{1/2})^2}{\sum_{u'v'} N_{u'v'}},$$

where $\hat{F}(\mu)_{uv} = \mathcal{F}(\hat{\mathbf{f}}(\mu))_{uv}$. For a large μ , the prior is strong and the error is large. As μ shrinks the error decreases, but more components of \mathbf{f} turn positive and $\hat{\mathbf{f}}(\mu)$ would be less clear. Thus, we stop decreasing μ just before the slope of $\text{error}_{\mathcal{F}}(\mu)$ becomes flat.

Shrinking μ also has a computational benefit. Generally, the MAP estimate for a large μ is computed easily and $\hat{\mathbf{f}}(\mu)$ is a good initial value for the algorithm with a slightly smaller μ . Another technique used to speed up the convergence was a simple line search of η_t in Eq. (5). It effectively accelerated the convergence.

Figure 3 shows the $\text{error}_{\mathcal{F}}(\mu)$ for the diffraction data in Fig. 2. The value of μ was varied from 1×10^4 to 1×10^{-2} . Note that the abscissa axis of the figure increases from left to right, but the value of μ was decreased in the experiments. It can be seen that the error slope becomes flat at $\mu = 0.2$ and $\mu = 0.3$ for 1.0×10^{21} and 5.0×10^{21} photons/pulse/mm², respectively.

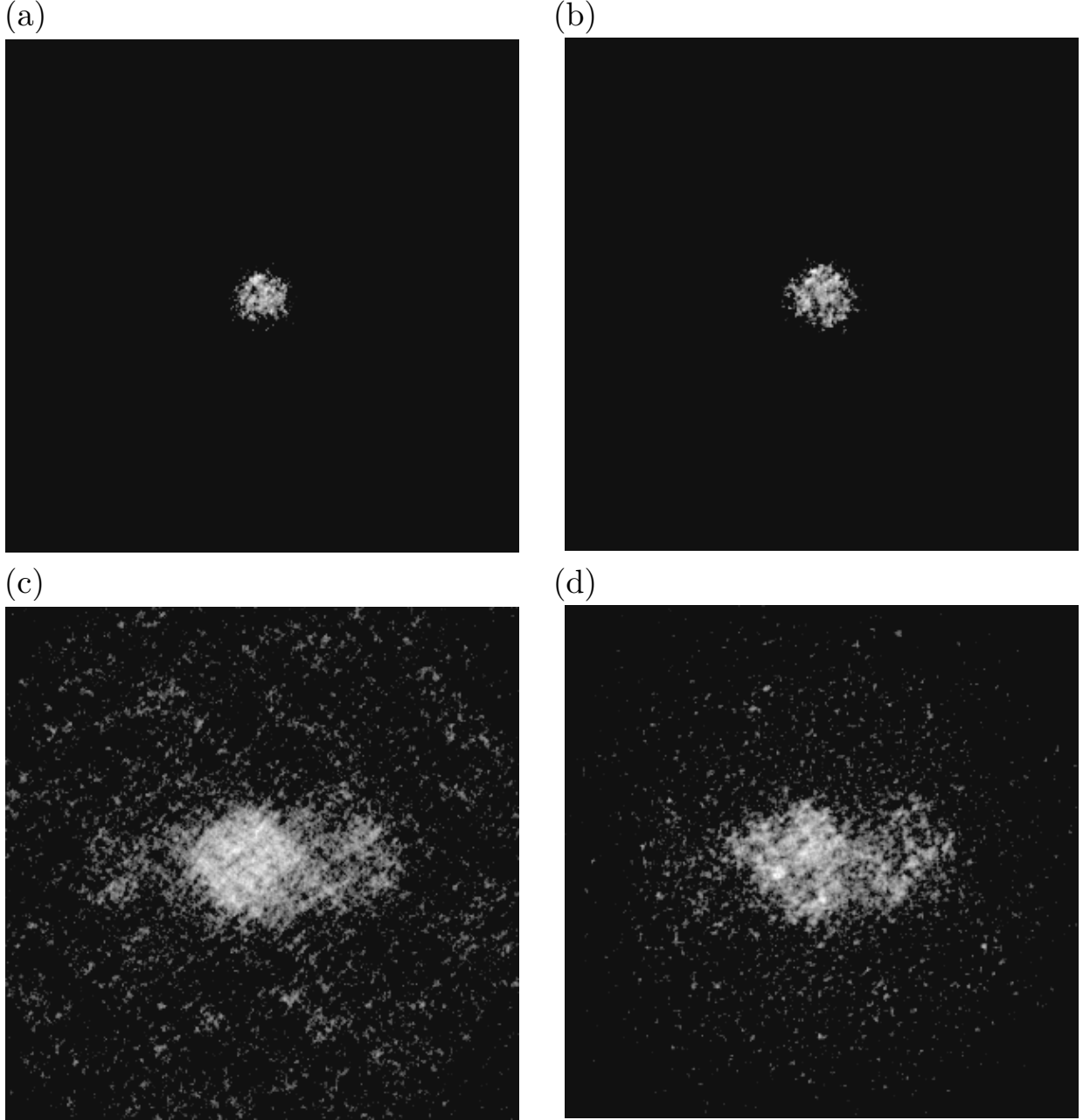


FIG. 4. Reconstructed density images with SPR method. (a) and (c) are for the diffraction image in Fig. 2(a), and (b) and (d) are for the diffraction image in Fig. 2(b). The values of μ were (a) $\mu = 100$, (b) $\mu = 100$, (c) $\mu = 0.3$, and (d) $\mu = 0.5$.

Two reconstructed densities for each diffraction data are shown in Fig. 4. Figures 4(a) and 4(c) are for the diffraction image in Fig. 2(a) and Figs. 4(b) and 4(d) are for that in Fig. 2(b), respectively. A larger value of μ ($\mu = 100$) makes the results sparser (Figs. 4(a) and 4(b)), and decreasing μ will reconstruct the whole density \mathbf{f} . The reconstructed densities

for the chosen μ 's are fairly good. This shows the SPR method is a promising method for the density reconstruction.

We have shown the SPR method for the density reconstruction or the phase retrieval of a single molecule diffraction. The method is based on the Bayesian statistics with a sparse prior and works reasonably well under very noisy situation.

The major differences between the SPR and conventional methods are summarized in two points. One is the error term. Widely used error measure is the squared loss, while the log-likelihood of a Poisson distribution is employed for the SPR method. Similar idea has been found in a related work [7]. This form is suitable for scattering data to be obtained experimentally, especially when the number of the scattered photons is very limited. The other point is the constraint. The SPR method poses the "soft constraint" with a prior distribution instead of the "hard constraint" with a support region. This is a new promising direction for phase retrieval.

Finally, we list some of our future works to improve the SPR. One is the hyperparameter. The hyperparameter $\rho(\mu)_{xy}$ can be modified to reflect the knowledge of the true density. This may result in a better estimate. Another issue is the algorithm. The densities for the whole sequence of μ in Fig. 3 were reconstructed with a few hours with MATLAB installed on a standard PC, but advanced optimization methods will speed up it.

We would like to thank Nobuhiro Go for fruitful discussion and Atsushi Tokuhisa for providing the electron density data and sharing the reconstruction results based on the HIO method. We are also grateful to Satoshi Ito for helpful discussion on the optimization method. This work was partly supported by X-ray Free Electron Laser Utilization Research Project of the Ministry of Education, Culture, Sports, Science and Technology of Japan.

-
- [1] D. Sayre, in *Imaging Processes and Coherence in Physics*, edited by M. Schlenker *et al.* (Springer, Berlin, 1980).
 - [2] K. Gaffney and H. Chapman, *Science* **316**, 1444 (2007).
 - [3] R. Neutze, R. Wouts, D. van der Spoel, E. Weckert, and J. Hajdu, *Nature* **406**, 752 (2000).
 - [4] G. Huldt, A. Szöke, and J. Hajdu, *J. Str. Biol.* **144**, 219 (2003).
 - [5] M. Seibert *et al.*, *Nature* **470**, 78 (2011).

- [6] L. Young *et al.*, Nature **466**, 56 (2010).
- [7] R. Irwan and R. G. Lane, J. Opt. Soc. Am. A **15**, 2302 (1998).
- [8] S. Baskaran and R. P. Millane, IEEE trans. Image Processing **8**, 1420 (1999).
- [9] J. Fienup, Applied Optics **21**, 2758 (1982).
- [10] J. Fienup, Optics Letters **3**, 27 (1978).
- [11] J. Miao, D. Sayre, and H. Chapman, J. Opt. Soc. Am. A **15**, 1662 (1998).
- [12] R. Tibishirani, J. R. Stat. Soc., Ser. B **58**, 267 (1996).
- [13] Personal communication with Dr. Atsushi Tokuhisa (RIKEN). The support region for HIO calculations was pre-defined as the central 154×154 pixels.
- [14] S. Marchesini *et al.*, Phys. Rev. B **68**, 140101 (2003).